

CDDIP: Constrained Diffusion-Driven Deep Image Prior for Seismic Image Reconstruction

Paul Goyes-Peñañiel¹, Ulugbek S. Kamilov², *Senior Member, IEEE*, Henry Arguello¹, *Senior Member, IEEE*,

Abstract—Seismic data frequently exhibits missing traces, substantially affecting subsequent seismic processing and interpretation. Deep learning-based approaches have demonstrated significant advancements in reconstructing irregularly missing seismic data through supervised and unsupervised methods. Nonetheless, substantial challenges remain, such as generalization capacity and computation time cost during the inference. Our work introduces a reconstruction method that uses a pre-trained generative diffusion model for image synthesis and incorporates Deep Image Prior (DIP) to maintain data consistency when reconstructing missing traces in seismic images. The proposed method has demonstrated strong robustness and high reconstruction capability for field and synthetic seismic images with different levels of structural complexity, even in scenarios where test images were outside the training domain. This indicates that our method can handle the high geological variability of different exploration targets. Additionally, compared to other state-of-the-art seismic reconstruction methods using diffusion models, our approach reduces the number of neural function evaluations by up to 4x. Our implementation is available at <https://github.com/PAULGOYES/CDDIP.git>

Index Terms—Seismic data reconstruction, diffusion models, deep image prior, seismic enhancement, consistent diffusion

I. INTRODUCTION

ENHANCING post-stack seismic images is crucial for reducing exploration risks, especially in conventional and unconventional energy sources such as geothermal energy, shale gas, and rock-based hydrogen. In seismic processing, post-stack images may exhibit missing or corrupted traces due to various factors such as equipment malfunction, data acquisition errors, incomplete coverage during data acquisition, signal attenuation, or interference from surface or subsurface features [1].

The reconstruction traces problem in the seismic context has been mainly addressed by methods based on deep learning, which can be primarily categorized into supervised and unsupervised learning paradigms [2]. Supervised learning methods predominantly rely on end-to-end models that necessitate large-scale datasets comprising pairs of corrupted images and their corresponding labels. These models' performance decreases when corrupt images are outside the training domain, common in subsurface exploration due to significant changes in geological formations and structural complexities based on

geographic location. To enhance the generalization capabilities of supervised learning models, efforts have been made to harness the strengths of generative models and integrate them into reconstruction learning frameworks [3]. On the other hand, schemes based on denoisers have been proposed, enabling reconstruction to be performed in a probabilistic fashion [4], [5]. Recently, seismic reconstruction has utilized unsupervised deep learning through Deep Image Prior (DIP) [6]–[8]. This methodology enables training a network solely with the measurements and inputting random noise. The approach capitalizes on the convolutional neural networks' capabilities to extract features from the seismic image and adapts the network to the measurements [7]. Thus, the need for extensive databases is alleviated, simplifying the reconstruction of traces in diverse geological settings independent of data availability. While DIP has demonstrated promising results in seismic data reconstruction, one of its main drawbacks is its reliance on overfitting noise towards the measurements. Therefore, DIP requires strict control over the number of epochs and the implementation of proper early-stopping techniques [9].

In the image restoration state-of-the-art, the probabilistic diffusion models [10] have played a key role [11]. For instance, [12] proposed denoising diffusion models for Plug-and-Play image restoration (DiffDPR) and solved the inverse problem with a closed-form solution given by [13]. Also, applications for Phase Retrieval [14] enforce the consistency of image generation with the measurements using a subgradient of the least-squares data-fidelity term. Specifically for seismic reconstruction, schemes that leverage diffusion models and closed-form solutions have been proposed to condition seismic data reconstruction and exploit generative models' capabilities [15]–[17]. However, in those studies, the reconstruction task was tested on data within the same training domain, and specifically in [16], the diffusion model was retrained for different datasets. This is a disadvantage due to the limited generalization of the reconstruction task.

This work presents a novel seismic reconstruction method using diffusion models with consistent sampling. The diffusion model is trained to generate samples from the posterior distribution by capturing the underlying structure of the seismic images. These diffusion samples represent a possible reconstruction of the missing traces. We employ a DIP solver instead of a closed-form solution to generate images constrained by partial measurements. Unlike closed-form solutions, DIP leverages convolutional neural networks to extract image features, enhancing the generalization capabilities of our approach. In addition, DIP acts as a prior distribution over the generated images from the diffusion model, enforcing consistency based on the observed traces. Consequently, we can reduce the number of diffusion steps needed to accurately reconstruct

Manuscript received July 24, 2024; revised Month 00, 000.

This work was funded by the Vicerrectoría de Investigación y Extensión from Universidad Industrial de Santander under Project 3925.

Paul Goyes-Peñañiel and Henry Arguello are with the Department of Systems Engineering, Universidad Industrial de Santander, Bucaramanga 680002, Colombia (e-mail: ypgoye@correo.uis.edu.co; henarfu@uis.edu.co)

Ulugbek S. Kamilov is with the Department of Computer Science and Engineering and Department of Electrical and Systems Engineering, Washington University in St. Louis, St. Louis, MO 63130, USA (e-mail: kamilov@wustl.edu)

missing traces by using scheduled steps to be denoised by the DIP.

II. PROPOSED METHOD

The reconstruction of seismic traces is an ill-conditioned problem that involves removing n traces (i.e., columns) from a post-stack seismic image $\mathbf{x} \in \mathbb{R}^{m \times n}$ with m time (or depth for Prestack Depth Migration) samples. In the view of computational imaging, the subsampled seismic image $\mathbf{y} \in \mathbb{R}^{m \times n}$ due to missing traces at positions \mathbf{j} can be modeled by a degradation model given by the following expression:

$$\mathbf{y} = \mathbf{M} \odot \mathbf{x} + \boldsymbol{\omega}, \quad (1)$$

where $\mathbf{M} = [\mathbf{m}_1, \mathbf{m}_2, \dots, \mathbf{m}_n] \in \{0, 1\}^{m \times n}$ is the subsampling/masking operator with \mathbf{m}_j denoting the j -th column of \mathbf{M} , and \odot is the element-wise multiplication, and $\boldsymbol{\omega}$ is the measurement noise. The structure of the non-zeros columns of \mathbf{M} determines the sampling scheme of the traces, and it can be uniform, irregular, or even custom-designed [18]. In general, \mathbf{m}_j can be expressed as

$$\mathbf{m}_j = \begin{cases} 0 & \text{if } j \in \mathbf{j} \\ 1 & \text{otherwise.} \end{cases} \quad (2)$$

for $j = 1, 2, \dots, n$

We propose to estimate \mathbf{x} using the denoising diffusion probabilistic model (DDPM) [10] and enforce consistency with the measurements \mathbf{y} through a Deep Image Prior (DIP) to improve the convergence of the reconstruction problem.

The detailed steps are shown in Algorithm (1), where the inputs are the pre-trained generative diffusion model ϵ_θ , measurements \mathbf{y} , the masking operator \mathbf{M} and some desired timestep schedule $\mathbf{t} = \{t_1, t_2, t_3, \dots, t_k\}$ where k is the number of diffusion steps for the reconstruction, note that $t_1 = T$ is the number of total diffusion steps during training, and $t_k = 1$ is always the last diffusion step. The timestep sequence \mathbf{t} can be scheduled in a linear, quadratic, or exponential sampling [12]. In step 1, the DIP solver's trainable parameters Θ are randomly initialized. In step 2, the first step is given by a random noise image with normal standard distribution $\mathcal{N}(0, \mathbf{I})$. From steps 3 to 8, the isotropic Gaussian noise is prepared to be used in step 9 to perform the unconditional diffusion sampling $\tilde{\mathbf{x}}_0^{(t_i)}$.

Although early diffusion steps $\tilde{\mathbf{x}}_0^{(t_i)}$ remain noisy, we leverage the capability of DIP to handle noise and estimate a clean version solely based on the measurements \mathbf{y} . Thus, the role of DIP in step 10 is to condition the generation of an image from DDPM via $\mathcal{G}_\Theta(\tilde{\mathbf{x}}_0^{(t_i)})$ in several sampling timesteps to ensure consistency with the measurements \mathbf{y} . Therefore, it is worth mentioning that our approach does not require closed-form solutions for the inverse problem. Conversely, our method uses the DIP solver, which requires a few epochs. The DIP solution gradually improves the image during each timestep of the denoising diffusion process. Moreover, DIP is designed as a warm-starting model that leverages parameters from the previous state solution.

In step 11, the regularized consistency $\mathcal{G}_\Theta(\tilde{\mathbf{x}}_0^{(t_i)})$ is back to the diffusion process, keeping the noise scheduled level for a

Algorithm 1 Deep Consistent Diffusion Sampling

Require: $\epsilon_\theta, \mathbf{y}, \mathbf{M}, \mathbf{t}$ timestep schedule

Ensure: Restored seismic image \mathbf{x}_1

- 1: **Initialize** \mathcal{G}_Θ with Θ randomly uniform
 - 2: Sample $\mathbf{x}_T \sim \mathcal{N}(\mathbf{0}, \mathbf{I})$
 - 3: **for** i **in** $1, 2, 3, \dots, N$ **do**
 - 4: **if** $t_i > 1$ **then**
 - 5: $\mathbf{z} \sim \mathcal{N}(0, \mathbf{I})$ ▷ Isotropic gaussian noise
 - 6: **else if** $t_i = 1$ **then**
 - 7: $\mathbf{z} = 0$ ▷ Last diffusion step
 - 8: **end if**
 - 9: Unconditional diffusion sampling
 - 10: DIP subproblem given \mathbf{y}

$$\Theta^* = \arg \min_{\Theta} \left\| \mathbf{M} \odot \mathcal{G}_\Theta(\tilde{\mathbf{x}}_0^{(t_i)}) - \mathbf{y} \right\|_2^2$$
 - 11: Data consistency regularized by DIP
$$\mathbf{x}_{t_{i+1}} = \sqrt{\bar{\alpha}_{t_{i+1}}} \mathcal{G}_{\Theta^*}(\tilde{\mathbf{x}}_0^{(t_i)}) + \sqrt{1 - \bar{\alpha}_{t_{i+1}}} \cdot \mathbf{z}$$
 - 12: **end for**
 - 13: **return:** \mathbf{x}_1
-

desired diffusion timestep using the traditional formulation of the forward process with a distribution given by

$$q(\mathbf{x}_{t_{i+1}} | \mathcal{G}_\Theta(\tilde{\mathbf{x}}_0^{(t_i)})) = \mathcal{N}(\mathbf{x}_{t_{i+1}}; \sqrt{\bar{\alpha}_{t_{i+1}}} \mathcal{G}_\Theta(\tilde{\mathbf{x}}_0^{(t_i)}), (1 - \bar{\alpha}_{t_{i+1}}) \mathbf{I}). \quad (3)$$

As a result of using Eq. (3), we can achieve the desired outcome by performing only a few sampling timesteps, also known as Neural Function Evaluations (NFEs) [19]. This is because the denoising objective depends on the DIP solver, which relies solely on the sampling sequence. Therefore, our method is only affected by the number of DIP steps. Fig. 1 summarizes the proposed scheme of diffusion steps. Notably, some steps are skipped because the DIP solver regularizes the unconditional denoised image $\tilde{\mathbf{x}}_0^{(t_i)}$ using \mathbf{y} , thus improving the diffusion process to a k timesteps.

III. SIMULATIONS AND EXPERIMENTS

A. Diffusion training

We trained the diffusion model with a cosine noise schedule given by $1 - \alpha$ from 10^{-4} to 0.02 and $T = 1000$ diffusion steps. We used 14398 images with size 128×128 during the training, which provides diverse seismic features, considering different geological scenarios and subsurface complexities from 6 databases, including synthetic and field surveys, as shown in Table I.

Implementation details: We split randomly the dataset into 90% for training and 10% for testing (Experiments I and II). The diffusion model ϵ_θ was trained for 5000 epochs, with a computation time of 6 days. For the DIP solver, an attention U-NET was used [26]. \mathbf{M} simulates irregularly random missing traces for all experiments. All the experiments were done with

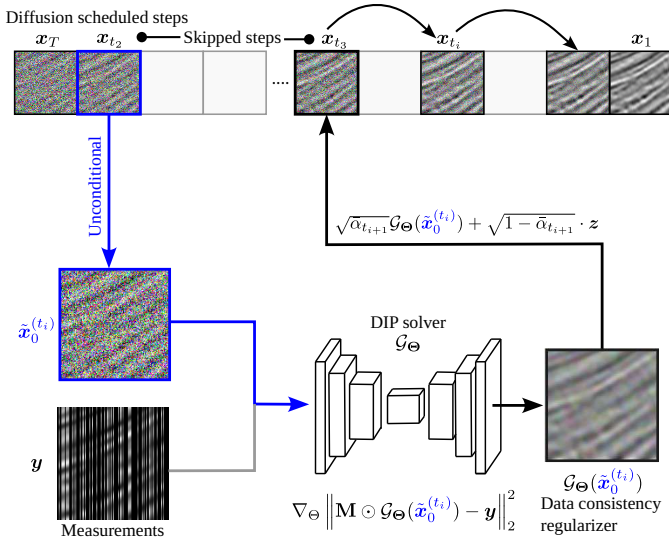


Fig. 1. Illustration with the conditional diffusion sampling. It is noteworthy how, between t_2 and t_3 , several steps of the pre-trained DDPM are skipped by using the DIP solver as a data consistency regularizer.

TABLE I
TRAINING DATASET SEISMIC IMAGES FROM (F) FIELD AND (S)
SYNTHETIC SURVEYS

| Dataset | #Training | Size (Mb) | |
|---------|--|-----------|------|
| S | TGS salt Identification challenge [20] | 4150 | 49.9 |
| | SEAM Challenge Phase 1 [21] | 4072 | 26.2 |
| | 1994 BP [22] | 803 | 4.15 |
| | AGL Elastic Marmousi [23] | 152 | 0.8 |
| F | F3 Netherlands [24] | 2000 | 15.9 |
| | Kerry 3D [25] | 3221 | 24.7 |
| Total | 14398 | 121.65 | |

an NVIDIA RTX 4090 24 GB GPU. Further implementation details are provided in the project repository.

B. Experiment 1

In this experiment, we analyze the impact of the number of timesteps k and DIP steps on the quality (PSNR and SSIM) of reconstructing 50% of the traces in a seismic image. The reconstruction results were compared to state-of-the-art methods that use conditional constraint diffusion models, namely DiffDPIR [12] and CCSeis-DDPM [15], [16]; for both methods, the diffusion model was trained with the same dataset reported in Table I. Table II shows that the lowest performance is obtained with 10 DIP steps. Additionally, regardless of the timestep value, increasing the number of DIP solver steps also improves the quality of the reconstructions. On the other hand, for $k = 25$ and $k = 50$ timesteps, increasing the number of DIP solver steps positively impacts the PSNR, which remains approximately around 37.19 dB on average. The visual results from Fig. 2 indicate that for smaller DIP steps, the solution is smoother, and as the steps increase, the solution adjusts more closely to the noise and curved seismic events (> 25 DIP steps).

It is essential to note that our method performs similarly to the CCSeis-DDPM and DiffDPIR methods. However, our

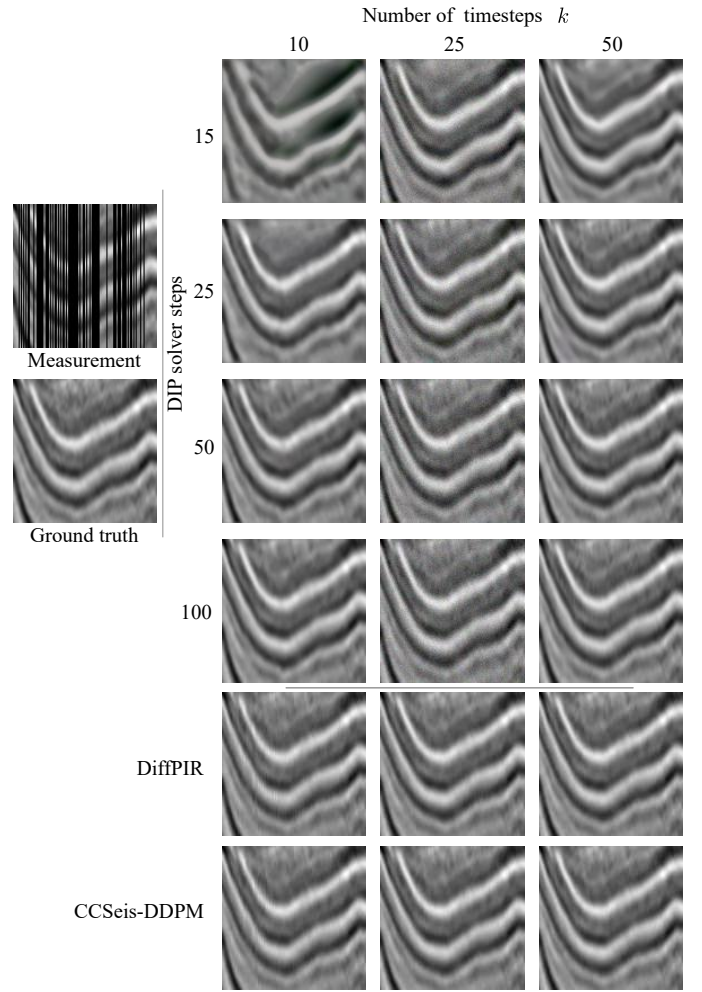


Fig. 2. Visual results of a seismic reconstruction experiment using a mask with 50% randomly missing traces for different DIP steps and sampling timesteps k with a linear/uniform schedule.

method handles internal measurement noise better. For example, Fig. 2 shows that reducing the number of DIP solver steps results in smoother reconstructions, whereas the other methods consistently produce noisy results.

TABLE II
QUANTITATIVE RECONSTRUCTION EVALUATION FOR DIFFERENT
DIFFUSION SAMPLING TIMESTEPS k AND DIP SOLVER STEPS

| Timesteps k | PSNR(dB) \uparrow | | | SSIM \uparrow | | | |
|---------------|---------------------|--------|---------------|-----------------|-------|-------|--------------|
| | 10 | 25 | 50 | 10 | 25 | 50 | |
| DIP steps | 15 | 21.624 | 33.194 | 33.804 | 0.497 | 0.861 | 0.874 |
| | 25 | 29.835 | 34.231 | 36.967 | 0.767 | 0.890 | 0.929 |
| | 50 | 34.024 | 37.190 | 37.058 | 0.892 | 0.930 | 0.937 |
| | 100 | 35.650 | 36.830 | 36.253 | 0.919 | 0.923 | 0.919 |
| DiffPIR | | 31.065 | 35.315 | 36.112 | 0.819 | 0.860 | 0.870 |
| CCSeis-DDPM | | 31.942 | 34.982 | 36.157 | 0.832 | 0.852 | 0.874 |

We found the best performance when using 50 DIP solver steps and $k = 25$, with an average computation time of 38 seconds. The comparison methods took 36 seconds on average. This provides a suitable balance between computation time and metrics evaluation. We remark that in other applications with less complex images, k could decrease.

C. Experiment II

In this experiment, we evaluate the reconstruction capability of our method over different seismic images containing linear and curved seismic structures and geological faults. Furthermore, the proposed approach enables the evaluation of reconstruction uncertainty by estimating diverse realizations. This is because diffusion sampling starts with random noise, which allows for the visualization of, for example, the spatial distribution of uncertainties using variance. This experiment uses $k = 25$ and 50 DIP solver steps.

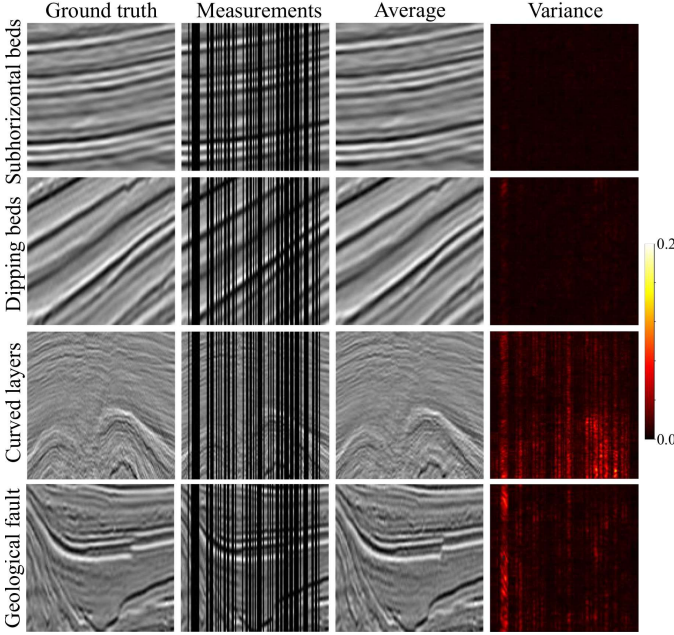


Fig. 3. Visual reconstruction results of the average and variance of five estimations using the proposed method with varying geological scenarios with 50% of missing traces. The four structural complexities increase from top to bottom rows.

In Fig. 3, our method accurately reconstructs lower structural complexity levels corresponding to subhorizontal and dipping beds, achieving PSNR values of 41.469 dB and 35.536 dB and SSIM values of 0.981 and 0.967, respectively. However, the method exhibits reduced performance for curved and highly noisy layers with a PSNR of 27.438 dB and SSIM of 0.741. This discrepancy arises because the employed DIP solver tends to generate smooth and noise-free images. Nevertheless, visually, our method captures the pertinent structural features of the seismic image. Our method maintains the original discontinuities and inclinations for seismic images depicting geological faults, obtaining a PSNR of 30.251 dB and SSIM of 0.849. Across all scenarios, variance values are high only for the image's left side, where 10 consecutive traces were removed.

D. Experiment III

This experiment aimed to assess the effectiveness of our method on data outside the training domain. In deep learning approaches, datasets are typically divided into training and testing subsets within the same domain. However, we sought to determine the efficacy of our approach when applied to

datasets entirely distinct from the training domain. The seismic datasets include Stratton, Penobscot, Black Ridge, and Alaska, each with unique complexities in image structures.

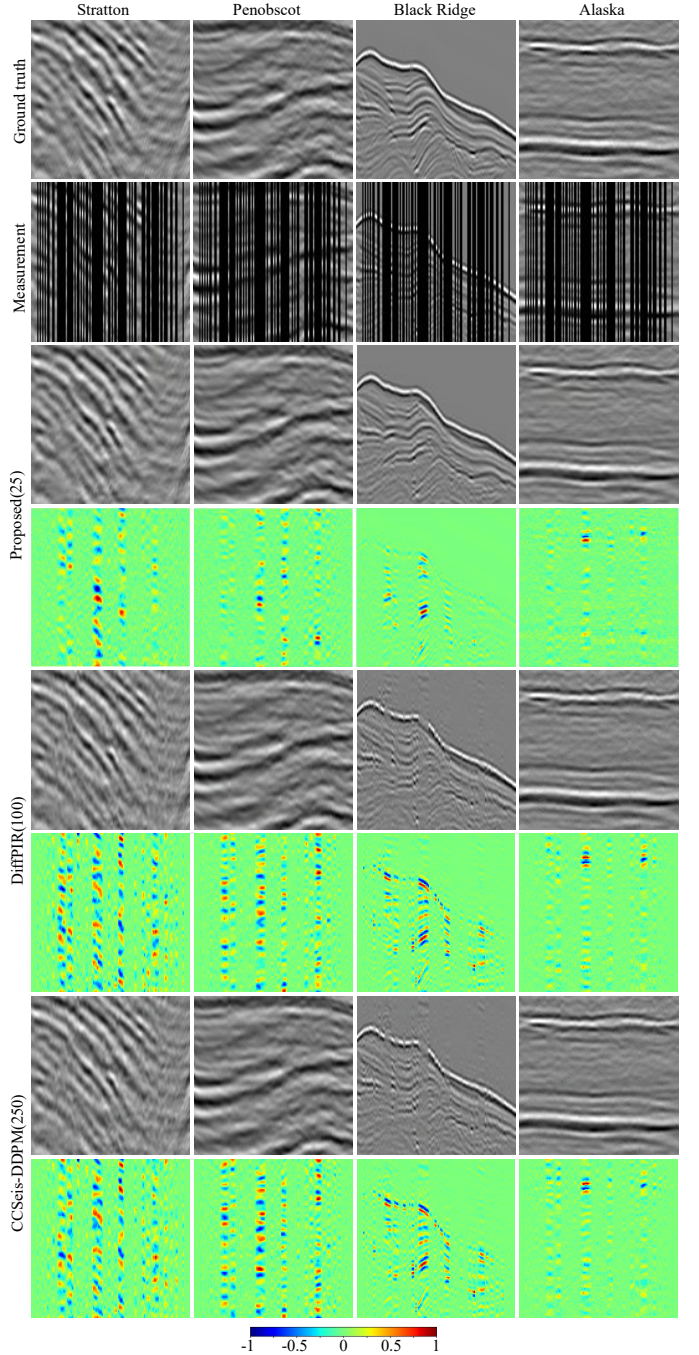


Fig. 4. Visual results depict the reconstruction of 60% missing traces using the proposed method, DiffPIR [12], and CCSeis-DDPM [15] with 25, 100, and 250 timesteps, respectively. For each method, the respective normalized error is presented below each reconstruction to highlight areas with the greatest discrepancies relative to the ground truth. It is noteworthy that the mask pattern remains consistent across all datasets.

This experiment uses $k = 25$ and 50 DIP solver steps for the proposed method. According to [12], [15], [16], we set k and U to 100 and 1 for DiffPIR, and 250 and 10 for the CCSeis-DDPM. U is the number of inner iterations within a timestep. Table III summarizes the metrics for each method across

different datasets. Notably, our method reduces the number of diffusion timesteps up to four times, allowing for investment in DIP solver steps. This increases generalization capability and eliminates the need for retraining, even when the application includes test data outside the training domain. Fig. 4 illustrates that, for the case of horizontal layers in the Alaska dataset, all methods achieved high performance exceeding PSNR 30 dB. However, our method performed better in reconstructing areas where consecutive traces were removed. While DiffPIR and CCSeis-DDPM generally demonstrated acceptable performance in the Black Ridge dataset, our method outperformed them by up to 2.2 dB in PSNR and 0.23 in SSIM, highlighting the effectiveness of the proposed method in complex scenarios.

TABLE III
AVERAGE QUANTITATIVE RESULTS FOR DIFFERENT SEISMIC SURVEYS.

| Dataset | Method | PSNR(dB) \uparrow | SSIM \uparrow |
|-------------|-------------|---------------------|-----------------|
| Stratton | Proposed | 28.664 | 0.797 |
| | DiffPIR | 25.697 | 0.689 |
| | CCSeis-DDPM | 25.653 | 0.691 |
| Penobscot | Proposed | 32.635 | 0.896 |
| | DiffPIR | 31.291 | 0.855 |
| | CCSeis-DDPM | 31.392 | 0.861 |
| Black Ridge | Proposed | 26.692 | 0.785 |
| | DiffPIR | 24.449 | 0.558 |
| | CCSeis-DDPM | 24.363 | 0.545 |
| Alaska | Proposed | 33.374 | 0.886 |
| | DiffPIR | 31.728 | 0.849 |
| | CCSeis-DDPM | 31.987 | 0.849 |

IV. CONCLUSIONS

This paper introduces a conditional diffusion model for seismic data reconstruction, leveraging DIP advantages to implement consistency in image synthesis from partial measurements during reverse diffusion. Our diffusion model was trained on field and synthetic datasets to learn the distribution of post-stack seismic images. Experiments demonstrated that our proposed method achieves outstanding results compared to state-of-the-art approaches in similar computation times. This holds for test data within the training domain, field data outside the training domain, and various complexities of seismic image structures related to different geological scenarios.

REFERENCES

- [1] Y. Tian, J. Gao, and D. Wang, "Improving seismic resolution based on enhanced multi-channel variational mode decomposition," *Journal of Applied Geophysics*, vol. 199, p. 104592, 4 2022.
- [2] T. Wu, X. Meng, H. Liu, and W. Li, "A seismic random noise suppression method based on self-supervised deep learning and transfer learning," *Acta Geophysica*, vol. 1, pp. 1–17, 6 2023.
- [3] P. Goyes-Penafiel, L. Suarez-Rodriguez, C. Correa, and H. Arguello, "Gan-supervised seismic data reconstruction: An enhanced-learning for improved generalization," 2023.
- [4] F. Wang, Z. Liu, F. Li, Q. Hu, and J. Ma, "Seismic data interpolation by learning a denoiser with deep implicit prior," *IEEE Geoscience and Remote Sensing Letters*, pp. 1–1, 2023.
- [5] M. Ravasi, "Probabilistic seismic interpolation with the implicit prior of a deep denoiser," *International Meeting for Applied Geoscience & Energy Expanded Abstracts*, pp. 970–974, 12 2023.
- [6] Q. Liu, L. Fu, and M. Zhang, "Deep-seismic-prior-based reconstruction of seismic data using convolutional neural networks," *GEOPHYSICS*, vol. 86, no. 2, pp. V131–V142, 3 2021.
- [7] F. Kong, F. Picetti, V. Lipari, P. Bestagini, X. Tang, and S. Tubaro, "Deep Prior-Based Unsupervised Reconstruction of Irregularly Sampled Seismic Data," *IEEE Geoscience and Remote Sensing Letters*, vol. 19, pp. 1–5, 2022.
- [8] L. M. Rodríguez-López, K. León-López, P. Goyes-Penafiel, L. Galvis, and H. Arguello, "Shot-gather Reconstruction using a Deep Data Prior-based Neural Network Approach," *Revista UIS Ingenierías*, vol. 22, no. 3, pp. 177–188, 9 2023.
- [9] Z. Xu and B. Wu, "Unsupervised deep learning seismic data random noise attenuation with early stopping," *Journal of Geophysics and Engineering*, vol. 20, no. 2, pp. 211–224, 2 2023.
- [10] J. Ho, A. Jain, and P. Abbeel, "Denoising Diffusion Probabilistic Models," in *Advances in Neural Information Processing Systems*, vol. 2020-Decem. Neural information processing systems foundation, 6 2020.
- [11] A. Lugmayr, M. Danelljan, A. Romero, F. Yu, R. Timofte, and L. Van Gool, "RePaint: Inpainting using Denoising Diffusion Probabilistic Models," in *Proceedings of the IEEE Computer Society Conference on Computer Vision and Pattern Recognition*, vol. 2022-June. IEEE Computer Society, 1 2022, pp. 11 451–11 461.
- [12] Y. Zhu, K. Zhang, J. Liang, J. Cao, B. Wen, R. Timofte, and L. Van Gool, "Denoising Diffusion Models for Plug-and-Play Image Restoration," in *IEEE Conference on Computer Vision and Pattern Recognition Workshops*, 5 2023, pp. 1–17.
- [13] K. Zhang, Y. Li, W. Zuo, L. Zhang, L. Van Gool, and R. Timofte, "Plug-and-Play Image Restoration With Deep Denoiser Prior," *IEEE Transactions on Pattern Analysis and Machine Intelligence*, vol. 44, no. 10, pp. 6360–6376, 10 2022.
- [14] S. Shoushtari, J. Liu, and U. S. Kamilov, "DOLPH: Diffusion Models for Phase Retrieval," in *57th Asilomar Conf. Signals, Systems, & Computers*, 11 2023, pp. 1–7.
- [15] F. Deng, S. Wang, X. Wang, and P. Fang, "Seismic Data Reconstruction Based on Conditional Constraint Diffusion Model," *IEEE Geoscience and Remote Sensing Letters*, vol. 21, pp. 1–5, 2024.
- [16] X. Wang, Z. Wang, Z. Xiong, Y. Yang, C. Zhu, and J. Gao, "Reconstructing Regularly Missing Seismic Traces With a Classifier-Guided Diffusion Model," *IEEE Transactions on Geoscience and Remote Sensing*, vol. 62, pp. 1–14, 2024.
- [17] R. Durall, A. Ghanim, M. R. Fernandez, N. Etrich, and J. Keuper, "Deep diffusion models for seismic processing," *Computers & Geosciences*, vol. 177, p. 105377, 8 2023.
- [18] A. Hernandez-Rojas and H. Arguello, "Design of Undersampled Seismic Acquisition Geometries via End-to-End Optimization," *IEEE Transactions on Geoscience and Remote Sensing*, vol. 62, pp. 1–13, 2023.
- [19] N. Elata, B. Kowar, T. Michaeli, and M. Elad, "Nested diffusion processes for anytime image generation," in *Proceedings of the IEEE/CVF Winter Conference on Applications of Computer Vision (WACV)*, January 2024, pp. 5018–5027.
- [20] A. Howard, A. Sharma, A. Lenamond, J. Adamck, M. McDonald, S. Kainkaryam, and W. Cukierski, "Tgs salt identification challenge," 2018. [Online]. Available: <https://kaggle.com/competitions/tgs-salt-identification-challenge>
- [21] M. Fehler and P. J. Keliher, *SEAM Phase 1: Challenges of Subsalt Imaging in Tertiary Basins, with Emphasis on Deepwater Gulf of Mexico*. Society of Exploration Geophysicists, 2011.
- [22] G. Sam and M. Kurt, "Migration from topography: Improving the near-surface image," 1995. [Online]. Available: https://wiki.seg.org/wiki/1994_BP_migration_from_topography
- [23] G. S. Martin, R. Wiley, and K. J. Marfurt, "Marmousi2: An elastic upgrade for marmousi," *The Leading Edge*, vol. 25, no. 2, pp. 156–166, 2006.
- [24] L. Baroni, R. M. Silva, R. S. Ferreira, D. Chevotarese, D. Szwarcman, and E. Vital Brazil, "Netherlands F3 interpretation dataset," Oct. 2018.
- [25] N. Z. C. Minerals, "Kerry 3D dataset," 1995. [Online]. Available: https://wiki.seg.org/wiki/1994_BP_migration_from_topography
- [26] O. Oktay, J. Schlemper, L. L. Folgoc, M. Lee, M. Heinrich, K. Misawa, K. Mori, S. McDonagh, N. Y. Hammerla, B. Kainz, B. Glocker, and D. Rueckert, "Attention u-net: Learning where to look for the pancreas," in *Medical Imaging with Deep Learning*, 2018. [Online]. Available: <https://openreview.net/forum?id=Skft7cijM>